ADVANCED MATERIALS INTERFACES
www.advmatinterfaces.de

Advanced Functional Hybrid Proton Exchange Membranes Robust and Conductive at 120 °C

*Jason Richard, Fatima Haidar, Madeline K. Alzamora, Manuel Maréchal, Natalia Rovira, Christophe Vacquier, Clément Sanchez, and Christel Laberty-Robert**

Proton-exchange membrane fuel cell vehicles offer a low-carbon alternative to traditional oil fuel vehicles, but their performances still need improvement to be competitive. Raising their operating temperature to 120 °C will enhance their efficiency but is currently unfeasible due to the poor mechanical properties at high temperatures of the state-of-the-art proton-exchange membranes consisting of perfluorosulfonic acid (PFSA) ionomers. To address this issue, xx designed composite membranes made of two networks: a mat of hybrid fibers to maintain the mechanical properties filled with a matrix of PFSA-based ionomer to ensure the proton conductivity. The hybrid fibers obtained by electrospinning are composed of intermixed domains of sulfonated silica and a fluorinated polymer. The inter-fiber porosity is then filled with a PFSA ionomer to obtain dense composite membranes with a controlled fibers-to-ionomer ratio. At 80 °C, these obtained composite membranes show comparable performances to a pure PFSA commercial membrane. At 120 °C however, the tensile strength of the PFSA membrane drastically drop down to 0.2 MPa, while it is maintained at 7.0 MPa for the composite membrane. In addition, the composite membrane shows a good conductivity of up to 0.1 S cm^{-1} at 120 °C/90% RH, which increases with the ionomer content.

1. Introduction

The global transport sector represents around 14% of global greenhouse gas emissions,[1] making it one of the main causes of global climate change. Important challenges concern optimization of performances of electrical vehicles, among which hydrogen fuel cell vehicles offer a low-carbon alternative to traditional oil fuel vehicles. Fuel cell vehicles rely on a fuel cell converting hydrogen or methanol into electricity. The current leading technology is the proton exchanging membrane fuel cell (PEMFC) operating with gaseous hydrogen and a proton-conducting membrane. It offers many benefits: good efficiency, reliability, and durability. However, the overall cost remains high and improvements in terms of performance and durability remain necessary to spread the technology. Two main strategies have been investigated so far: one concerns the design and development of cheaper efficient catalysts as Pt/Molybdenum carbides;[2] the other second attractive solution is to operate the PEMFC at high temperatures, which would simplify the heat management, increase the efficiency, improve the mass transport and greatly limit the catalyst poisoning by carbon monoxide.[3] An operating temperature of 120 °C was set by the U.S. department of energy for PEMFC operation. However, the state-of-the-art proton exchange membranes (PEM) consisting of perfluorosulfonic acid (PFSA) polymers, considered benchmark materials, have poor mechanical and conductive properties that greatly reduce their efficacy at $T > 100$ °C, which limits the operating temperature.

Over the last two decades, the scientific community has proposed many strategies to enhance PEM performances at high

J. Richard, F. Haidar, M. K. Alzamora, C. Sanchez, C. Laberty-Robert
Laboratoire Chimie de la Matière Condensée de Paris LCMCP
Sorbonne Université
UPMC Paris 06, 4 Place Jussieu, Paris 75005, France
E-mail: christel.laberty@sorbonne-universite.fr
J. Richard, C. Sanchez
Collège de France
Laboratoire Chimie de la Matière Condensée de Paris
UMR-CNRS 7574 4 place Marcelin Berthelot, Paris 75005, France
The ORCID identification number(s) for the author(s) of this article can be found under https://doi.org/10.1002/admi.202201601.

DOI: 10.1002/admi.202201601

M. Maréchal
Univ. Grenoble Alpes
CNRS
CEA
IRIG-SyMMES
Grenoble 38000, France
N. Rovira, C. Vacquier
Symbio
5 Rue Simone Veil, Vénissieux 69200, France
C. Sanchez
USIAS University of Strasbourg, Institute of Advanced Study
5 allée du Général Rouvillois, Strasbourg 67083, France
C. Laberty-Robert
RS2E
Réseau Français sur le Stockage Electrochimique de l'Energie
CNRS 3459, Cedex 1 Amiens 80039, France

temperatures: developments of new sulfonated polymers,[4–7] combination of acid and base functions,[8–10] hybridization with hydrophilic inorganic particles[11,12] or metal-organic frameworks,[13] reinforcement with PTFE,[14,15] altogether with other approaches. One of the most promising strategies to enhance the membrane's performance is to design composite membranes by the incorporation of metal oxide particles into a PFSA matrix.[16–18] While this method is showed to enhance the water retention and the hardness of the membrane at moderate temperatures, the poor stability of the oxide/Nafion interfaces leads to a decrease in the performance of the membrane with RH cycling.[19] Moreover, the brittleness of the membrane increases with the inorganic content, which may be detrimental to the mechanical properties.[3] Another approach was developed by T. Yogo and col. who synthesized hybrid membranes by copolymerization of purely organic monomers and monomers containing siloxane or silsesquioxane functions.[20–22] In this case, no organic and inorganic domains exist, but rather a homogeneous matrix made of covalent C—C, C—Si and SiO—Si bonds. They reported tensile strength of up to 12 MPa at room temperature but did not investigate the mechanical properties at higher temperatures.

Among the various methods to obtain composite membranes, electrospinning offers the possibility to incorporate nanosized inorganic domains homogeneously dispersed in polymer nanofibers. Liu et al.[23] reported the synthesis of an electrospun PVDF mat which was post- functionalized by dip-coating to form hybrid PVDF-SiO_2 nanofibers. Sulfonic acid functions were grafted onto the silica and the mat porosity was filled with chitosan, obtaining a membrane whose proton conductivity reached 0.044 S cm^{-1} at 80 °C. In their work, Wang et al.[24] reported the synthesis of a composite mat made of amino-modified SiO_2 nanoparticles imbedded in sulfonated poly(ether sulfone) nanofibers, which was further impregnated with a perfluorosulfonic ionomer. In this case, the silica particles were first obtained via a modified Stöber process and then mixed with the polymer precursor solution. Obtained membranes exhibited a high proton conductivity of 0.23 S cm^{-1} at 80 °C in water. Similarly, Mojarrad et al.[25] reported the synthesis of poly(vinylidene fluoride-co-trifluoroethylene) electrospun fibers incorporating sulfonated mesoporous silica nanoparticles which reached a proton conductivity of 0.102 S cm^{-1}. These examples highlight the crucial importance of the method used to form and disperse the silica domains in the polymer fibers, which influences the morphology of the former as well as the polymer-silica interactions and thus the final performances of the membrane. However, these approaches involve many steps of synthesis, which may limit their industrial development.

Our group proposed to combine electrospinning and sol-gel chemistry as a direct strategy to obtain silica and polymer domains intermingled at the nanoscale.[26–28] In this method, the organo-silica network is formed in situ during the electrospinning process through sol-gel chemistry in acidic conditions. This contrasts with other reported works on hybrid nanofibers in which the silica is condensed in alkali conditions and leads to a clearly defined phase separation with the polymer, that is, with silica particles within or onto the polymer fibers.[23–25] On the contrary, our approach forms interpenetrated networks of a hydrophobic fluorinated polymer and hydrophilic sulfonated silica along the fibers. This specific organization should also avoid the leaching of the inorganic part during wet/dry cycles. In the following works, we studied the influence of the composition of the nanofibers on the proton conductivity[29] and further investigated the mechanism of the proton transport in dry[30] and wet states.[31] However, the electrospun mats had inter-fibers porosity, which may lead to fuel crossover during the fuel cell operation; in addition, the properties at $T > 80$ °C were not investigated. Here, we propose to control the porosity via hot-pressing and study its influence on the conductivity of the membrane. To further densify and improve the performances of the membrane, the remaining porosity is filled with a proton conductive ionomer and obtained composite membranes are characterized at 80 and 120 °C.

In this study, we aim to design a hybrid nanostructured membrane efficient at 120 °C. Our strategy is to form two networks: one to maintain the mechanical properties, and another to ensure the proton transport. The first network consists of hybrid nanofibers made of intermingled PVDF-HFP and sulfonated silica domains at the nanoscale. The second network is a PFSA ionomer infiltrated into the mat to fill the inter-fibers porosity. First, the optimization of the hybrid nanofibers' stability is presented in terms of formulation, structure, and porosity. Composite nanofibers/ionomer membranes are then obtained through impregnation with precise control of the fibers to ionomer volume ratio. At 80 °C, the best composite membrane has comparable performance to a commercial PFSA membrane (Nafion 212). At 120 °C, the tensile strength of the PFSA membrane drops to less than 0.2 MPa. On the opposite, the composite membrane maintained excellent mechanical stability and a showed tensile strength 35 times higher, as well as a good conductivity. These remarkable properties are assigned to the specific structure and ultrastructure of the hybrid nanofibers with a continuous silica organization along the fibers. Our results are discussed in the frame of the performances of other hybrid nanofibers-based PEM reported in the literature.

2. Results and Discussion

2.1. Hybrid Proton Exchange Membrane

Hybrid Proton Exchange Membranes (HPEM) were directly synthesized by electrospinning of a mixture of poly(vinylidene fluoride-co-hexafluoropropylene) (PVDF-HFP) and silica precursors (**Scheme 1**). Tetraethyl orthosilicate (TEOS) and chlorosulfonylphenyl-ethyl trichlorosilane were hydrolyzed in situ with the PVDF-HFP in acidic conditions and condensed during the electrospinning process to form silica domains functionalized by sulfonic acid functions.[31] The obtained membrane, called HPEM hereafter, is flexible and easy to handle. At the microscale, scanning electron microscopy (SEM) images show that it is composed of a mat of beads-free nanofibers (**Figure 1**a). The fibers present a homogeneous texture without the formation of discrete silica particles onto or between the fibers, which points toward a homogeneous distribution of

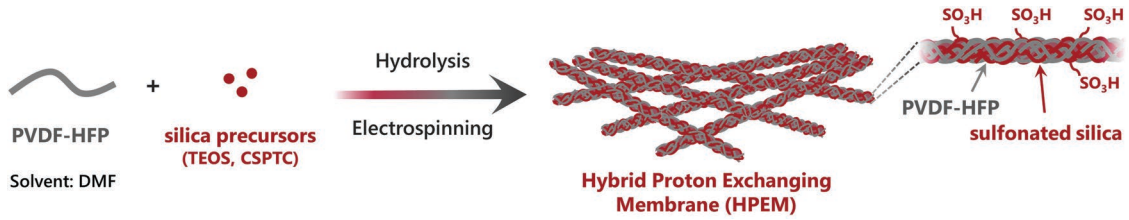

Scheme 1. Scheme of the synthesis process of Hybrid Proton Exchange Membrane (HPEM).

the polymer and the silica domains within the fibers. This homogeneity is further supported by the energy dispersive X-ray (EDX) mapping showing the distribution of fluorine, silicon, and sulfur elements (Figure 1a). Moreover, the density of sulfonic function measured by micro elemental analysis reaches 1.86 $mmol_{SO3H}$ g^{-1} (**Table 1**). Up to 82% of these acidic protons are accessible to ionic exchange, with a high ionic exchange capacity (IEC) of 1.53 $mmol_{H+}$ g^{-1} measured by acid-base titration after an exchange in a sodium chloride solution. Noteworthy, these values exceed those of commercial PFSA membranes (IEC of 0.9–1.2 $mmol_{H+}$ g^{-1})[32] and those of similar materials reported in the literature.[28,33]

The proton conductivity of HPEM at 80 °C versus the relative humidity (RH) is shown on Figure 1b. The conductivity increases from $1.8.10^{-4}$ S cm^{-1} at 20% RH to $2.6.10^{-2}$ S cm^{-1} at 100% RH, indicating that water molecules are involved in the proton migration mechanism. The nano-scale organization of HPEM fibers were investigated by small angle X-ray scattering (SAXS) at 0%, 50%, and 100% RH from 80 to 120 °C; selected curves are shown in Figure 1c (all curves are given in Figure S1, Supporting Information). All SAXS curves present two contributions at around 0.7 and 3 nm^{-1} characterizing the characteristic distances between PVDF-HFP rich domains and between ionic sulfonate functions, respectively. The corresponding mean distance between PVDF-HFP domains is around 9 nm which also corresponds to previously reported measurements.[34,35] In addition, a short and steady average interionic distance of 2.1 nm was found from 0 to 100% RH and from 80 to 120 °C, showing a highly stable and dense ionic network. This stability likely comes from the inorganic nature of the ionic domains, that is, the functionalized silica.

The upturn in intensity at low scattering vectors, commonly interpreted as an inhomogeneity at the scale of several hundreds of nanometers, can be attributed to the scattering of the heterogeneous distribution of the subdomains. Specifically, the $I = f(q)$ curves follow an $I \propto q^{-\alpha}$ law, with the α parameter being characteristic of the geometry of the interfaces between hydrophobic and hydrophilic domains, that is, polymer and silica domains.[23] For HPEM, $\alpha = 3.1 \pm 0.1$ for all temperatures and humidity, which describes rough or fractal interfaces

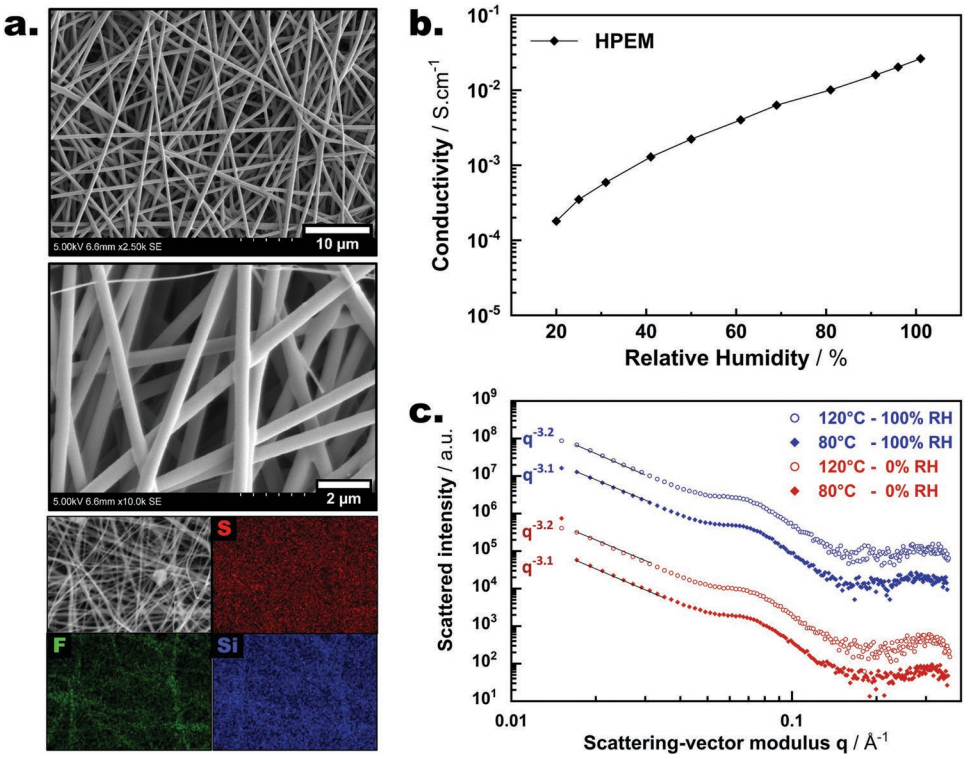

Figure 1. Properties of electrospun hybrid proton exchanging membrane: a) SEM images and EDX mapping; b) evolution of proton conductivity with relative humidity at 80 °C; c) selected SAXS curves at 80 and 120 °C, 0% RH and 100% RH.

Table 1. Morphological and chemical parameters of hybrid proton exchange membranes with or without PEG used as an additive.

	Fibers diameter [nm]	Sulfur content[a)] [mmol g^{-1}]	Ion exchange capacity[b)] [$mmol_{H+}$ g^{-1}]
HPEM	760 ± 120	1.86	1.53

[a)]Total sulfur content measured by elemental analysis; [b)]IEC measured by acid-base titration after an exchange in an aqueous solution of NaCl.

between silica and polymer consistently with interpenetrated networks.[31] It is noteworthy that such morphology should prevent the leaching of the silica, as it has been observed for Li-ion battery separators functionalized with silica particles.[36,37] This specific organization of silica domains comes from the acidic conditions and low H_2O/Si ratio of the in situ hydrolysis-condensation process, as described by Brinker.[38] The constancy of α shows highly stable interfaces, even at 120 °C and 100% RH.

Poly(ethylene glycol) (PEG) was added into the formulation to tune de PVDF-HFP/SiO_2 interfaces and optimize the transport of proton by the addition of hydrophilic functions. HPEM-PEG refers to the membrane synthesized with PEG and was fully characterized by elemental analyses, EDX, SEM, SAXS, and conductivity measurements. All results are described and discussed in detail in Section S2, Supporting Information. To sum up the investigations, the addition of PEG: i) decreases the density of ionic functions and increases their mean correlation distance; and ii) makes the nanofibers' conductivity and organization at the nanoscale more sensitive toward the humidity and the temperature. These effects may come from the incorporation of the hydrophilic PEG chains into the silica domains or at the silica/PVDF-HFP interface. Our target being the design of a PEM efficient at elevated temperatures, we chose to focus on HPEM without PEG for the rest of this work.

2.2. HPEM Porosity

For fuel cell applications, dense membranes are required to avoid fuel crossover; hence, the porosity of HPEM was controlled after synthesis using a laminar press. Initial pristine HPEM has a high porosity of 86% resulting from the large inter-fibers porosity. Applying pressures between 10 and 20 MPa and temperatures from 80 to 90 °C, the porosity of the membranes was controlled in the range of 86% to 50% (**Table 2**). The corresponding membranes' densities range from 0.29 to 1.02 g cm^{-3}, respectively. SEM images of obtained membranes in **Figure 2**a show that the pressing greatly reduced the inter-fiber porosity. Although the fibers were slightly flattened, they did not melt and merge because the applied temperature was below the melting temperature of PVDF-HFP ($T_m \approx 125$ °C).[39] Thus, some macroporosity remains visible between the stacked fibers.

Table 2. Porosity of the different hybrid PEM depending on the pressing conditions (laminar press, press time 10 min, 3 measurements on each membrane).

Sample	Pressing	Porosity	Density [g cm^{-3}]
HPEM – ε_p = 86%	Unpressed	86% ± 1%	0.29 ± 0.01
HPEM – ε_p = 70%	80 °C, 10 MPa	70% ± 2%	0.60 ± 0.03
HPEM – ε_p = 59%	80 °C, 15 MPa	59% ± 2%	0.83 ± 0.04
HPEM – ε_p = 50%	90 °C, 20 MPa	50% ± 2%	1.02 ± 0.05

The proton conduction of the HPEM membranes with controlled porosities was then studied at 80 °C and compared to a commercial perfluorosulfonic acid-based membrane, Nafion NRE212 (Figure 2b). The shape of all HPEM curves is similar, which indicates similar proton transport behaviors that are likely due to the preservation of the properties of the fibers during the pressing. However, the values of conductivity changed: the lower the porosity of the HPEM, the higher its conductivity. This can logically be interpreted by a geometrical factor, the same volume of conductive fibers being in a lower volume of the membrane. To investigate further this relationship between HPEM porosity and conductivity, the conductivity at 80 °C was studied as a function of porosity with fixed RH (Figure 2c and Figure S3, Supporting Information). Data points were fitted with a good agreement ($R^2 > 0.99$) using an exponential function:

$$\sigma_{80^\circ C} = \sigma^0_{80^\circ C} \times e^{-k\varepsilon_p} \quad (1)$$

with ε_p standing for the porosity of the membrane, k a constant, and a pre-factor $\sigma^0_{80^\circ C}$ corresponding to the theoretical value for a HPEM membrane without porosity. Thus, when the porosity decreases, the density of the fibers linearly increases but the conductivity exponentially increases. This relationship may arise from the formation of new contact points between the fibers after pressing, playing an active role in the continuum of the proton conductive pathways across the membrane. Furthermore, the values of $\sigma^0_{80^\circ C}$ were estimated for each relative humidity to deduce the theoretical conductivity of a perfectly dense HPEM (Figure 2d). HPEM-0% largely surpasses Nafion's performances at any RH with outstanding conductivities up to 1.8 S cm^{-1}. However, these values remain theoretical and come from the extrapolation of the conductivities of porous membranes and should be taken cautiously; some deviations could appear due to a modification of water uptake for instance. Anyhow, some porosity remains in the obtained membranes and can be used otherwise to create new proton conduction pathways.

2.3. HPEM-Ionomer Composite

Composite membranes were designed via a one-step impregnation of HPEM with perfluorosulfonic acid ionomer solution (**Figure 3**a). Obtained composite membranes have a smooth surface, with the inter fibers' porosity filled by the ionomer (Figure 3b). Varying the initial porosity ε_p of the HPEM from 55% to 86%, we were able to control the final volume ratio of ionomer to hybrid fibers α_i from 43% to 66% (Figure 3c). Moreover, we found a linear relationship between α_i and ε_p with a slope of 1, indicating that the porosity is effectively filled by ionomer through this simple process. The line intercepts the

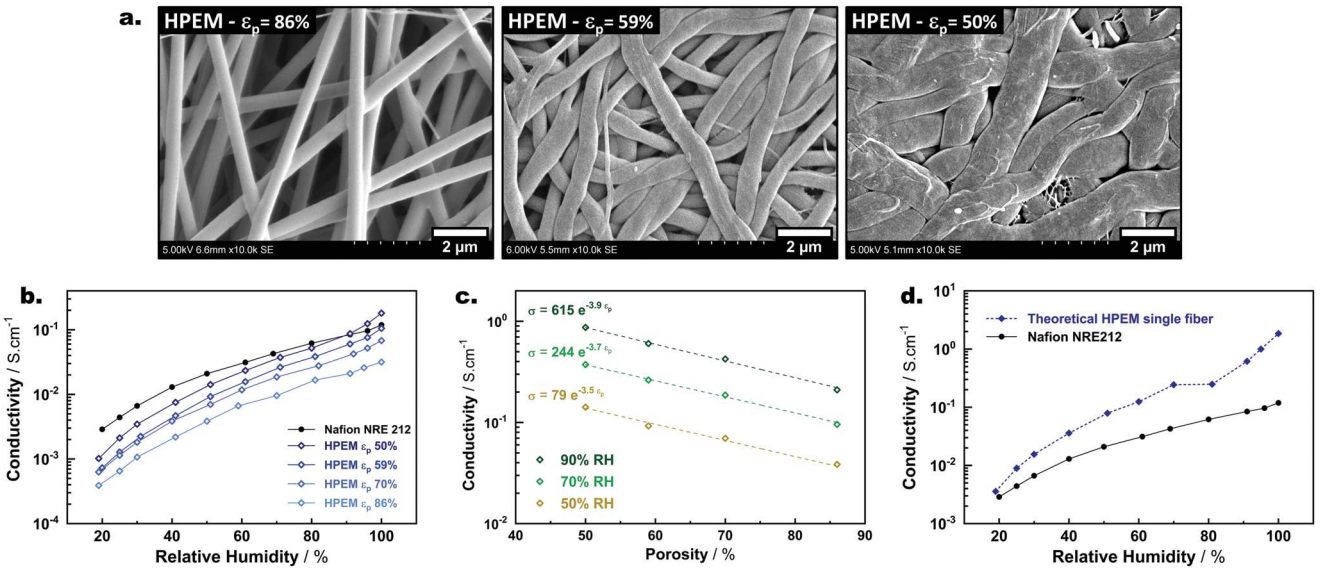

Figure 2. Properties of pressed HPEM according to their porosity ε_p: a) SEM images; b) evolution of proton conductivity with relative humidity at 80 °C; c) evolution of proton conductivity with ε_p at 80 °C; d) extrapolated conductivities for a perfectly dense HPEM versus relative humidity at 80 °C.

X-axis at ε = 21%, suggesting that some porosity is not filled with Nafion. It seems unlikely that some macroporosity is inaccessible by the ionomer solution because the wettability is excellent (immersed membranes become fully transparent). The remaining porosity thus likely comes from either the evaporation of the solvent during the one-step impregnation process[40] or the capillary effect that impedes complete impregnation.

The conductivities of all the composite HPEM-ionomer membranes were measured at 80 °C (**Figure 4**a). Surprisingly, the obtained performances did not vary much with the ionomer to fibers ratio. This suggests that both HPEM fibers and ionomer comparably participate in the overall transport, which would otherwise be correlated to either HPEM or ionomer content. To further understand the role of each component in the

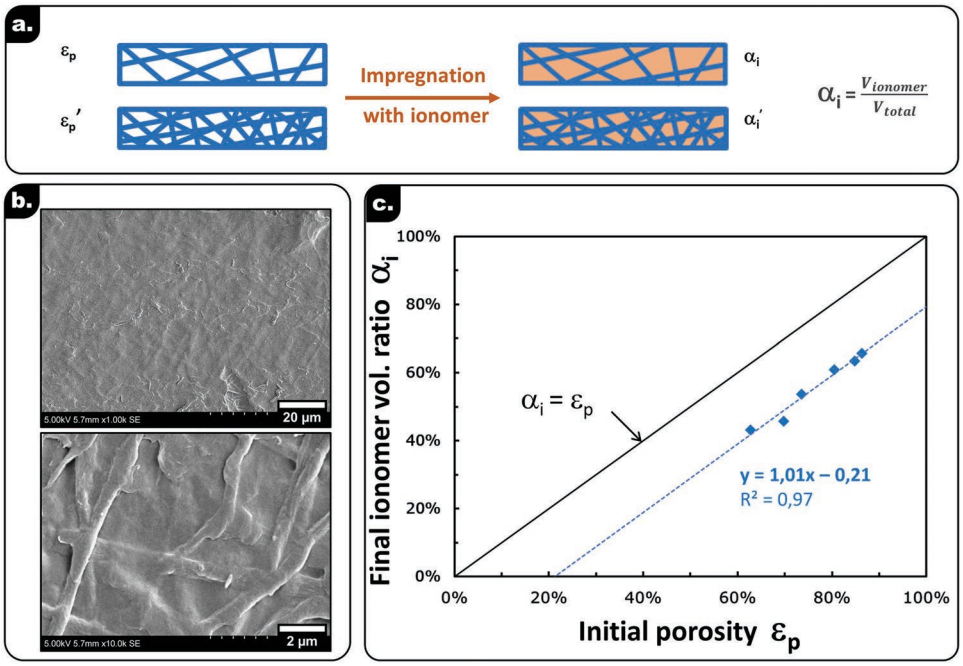

Figure 3. Design of HPEM-ionomer composite by impregnation: a) scheme of the process; b) SEM images of a HPEM-ionomer composite; c) final ionomer volume ratio in composites membrane depending on the initial porosity of hybrid membranes.

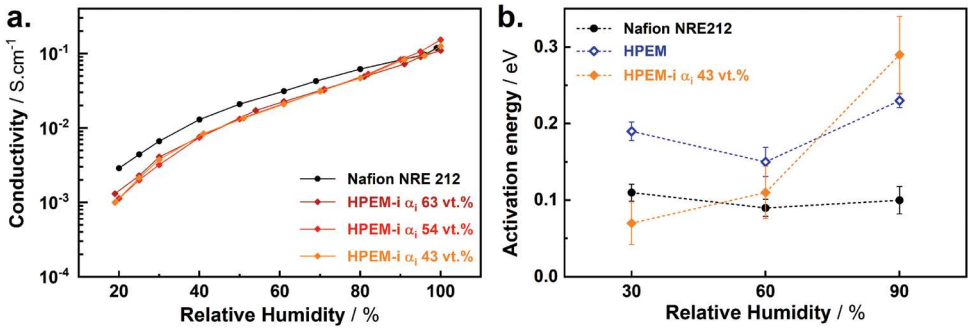

Figure 4. Conduction properties of HPEM-ionomer composites. a) Evolution of proton conductivity with relative humidity at 80 °C. b) Evolution with humidity of activation energy for calculated from Arrhenius equation.

transport of protons, we calculated the apparent activation energies E_a for pure HPEM, pure ionomer (Nafion NRE212), and HPEM-ionomer composites at 30%, 60% and 90% RH. The proton conductivity was first measured between 40 and 100 °C for each membrane and RH; E_a was then extrapolated from Arrhenius plots (see Figure S4, Supporting Information). For Nafion, we measured a value of $E_a = 0.10 \pm 0.01$ eV which was independent of RH on the studied range and corresponded to values reported for Nafion membranes in a hydrated state.[41,42] For HPEM, the activation energy was higher with a value of $E_a = 0.19 \pm 0.04$ eV, yet is also consistent with a Grotthuss transfer mechanism ($E_a < 0.40$ eV).[43] Concerning the HPEM-ionomer composite, the activation energy drastically increases with RH from 0.07 eV at 30% RH up to 0.39 eV at 90% RH. Notably, the obtained value at 30% RH matches the one of Nafion, while the activation energy at 90% RH matches the one of HPEM. It suggests that in HPEM-ionomer composite membranes, the ionomer appears to be the main conductor at low RH whereas HPEM fibers seem to be the main conductor at high RH. This would be consistent with their respective performances, since Nafion is more conductive than HPEM at low RH but less conductive at high RH.

Finally, we compared the proton conduction and mechanical performances of pure ionomer, pure HPEM, and HPEM-ionomer composites membranes at 120 °C. For Nafion, the conductivity at 120 °C exhibited the same trend with RH as at 80 °C, but with values 60% higher due to the activation of transport by the temperature (**Figure 5**a). However, the membrane sample after analysis turned yellow and was deformed, indicating poor stability of the ionomer at this temperature. Surprisingly, the pure HPEM membrane showed negligible conductivity at 120 °C. This result was unexpected given the high conductivity at 80 °C and the good stability of the fibers' organization observed by SAXS. It can be explained by the large fibers/air interface due to the morphology of the nanofibers, which makes the functionalized silica domains at the surface of the fibers more sensitive toward hydrolytic degradation. To support this hypothesis, a hydrothermal stability test was performed on a sample of HPEM membrane (Section S5, Supporting Information). XPS analyses confirmed the decrease of Si and S relative amounts at the surface of the fibers, which is consistent with the loss of $-SO_3H$ or $-$Si$-$OH functions. Still, FTIR-ATR analyses revealed that SO_3H and Si$-$O$-$Si moieties were still present in the material after the test, probably due to the presence of unaltered sulfonated silica domains within the fibers. In contrast, the HPEM-ionomer composite membranes present a proton conductivity at 120 °C that increases with the ionomer content. Yet, the conductivities remain somewhat lower than that of Nafion. At 120 °C/90% RH for instance, the conductivities of HPEM-i 66 vol% and Nafion are 0.10 and 0.16 S cm^{-1} respectively.

The major advantage of composite HPEM-ionomer membrane over Nafion is the drastic enhancement of the mechanical properties. Stress–strain tests were performed on HPEM, Nafion and HPEM-ionomer composite membranes (typical raw curves are shown in Figure S6, Supporting Information), and the measured Young's modulus and ultimate tensile strengths are reported in Figure 5b,c. At 80 °C, HPEM is stiffer than Nafion with Young's modulus of 110 and 41 MPa respectively. The composite HPEM-ionomer with 51 vol% of ionomer has a Young modulus of 133 MPa which is similar to the HPEM membrane, showing that the HPEM fibers act as an effective mechanical reinforcement. At 120 °C, Nafion is very soft as indicated by the severe decrease of its Young's modulus down to 1.5 MPa, causing a creep deformation of the membrane. In addition, the ultimate tensile strength becomes derisory with a value of only 0.2 MPa. This loss of mechanical performance is due to a temperature transition of Nafion in the 100–150 °C range, sometimes assigned to the glass transition temperature of the ionic regions.[44,45] On the contrary, both HPEM and HPEM-ionomer membranes stay rigid at 120 °C with almost no change in their Young's modulus compared to 80 °C. Noteworthy, the Young's modulus of HPEM-i $\alpha_{i\,=\,51\%}$ is 141 MPa, which is 95 times higher than the one of Nafion at the same temperature. Similarly, the ultimate tensile strengths of HPEM and HPEM-ionomer membranes remain high at 120 °C, with values of 9.9 and 7.0 MPa, which are 50 and 35 times higher than Nafion, respectively. These excellent performances come from the specific nanostructure of the fibers with intermingled domains of silica and polymer evidenced by SAXS. More specifically, it can be stated that the silica forms a continuous percolated network along the fibers, which maintains the mechanical properties even close to the melting point of the PVDF-HFP. As an illustration, a sample of HPEM membrane was ignited with a blowtorch; the sample remained in one piece after burning. Consequently, the composite HPEM-ionomer membrane offers an excellent overall compromise at 120 °C: while the electrospun fibrous hybrid mat maintains outstanding mechanical

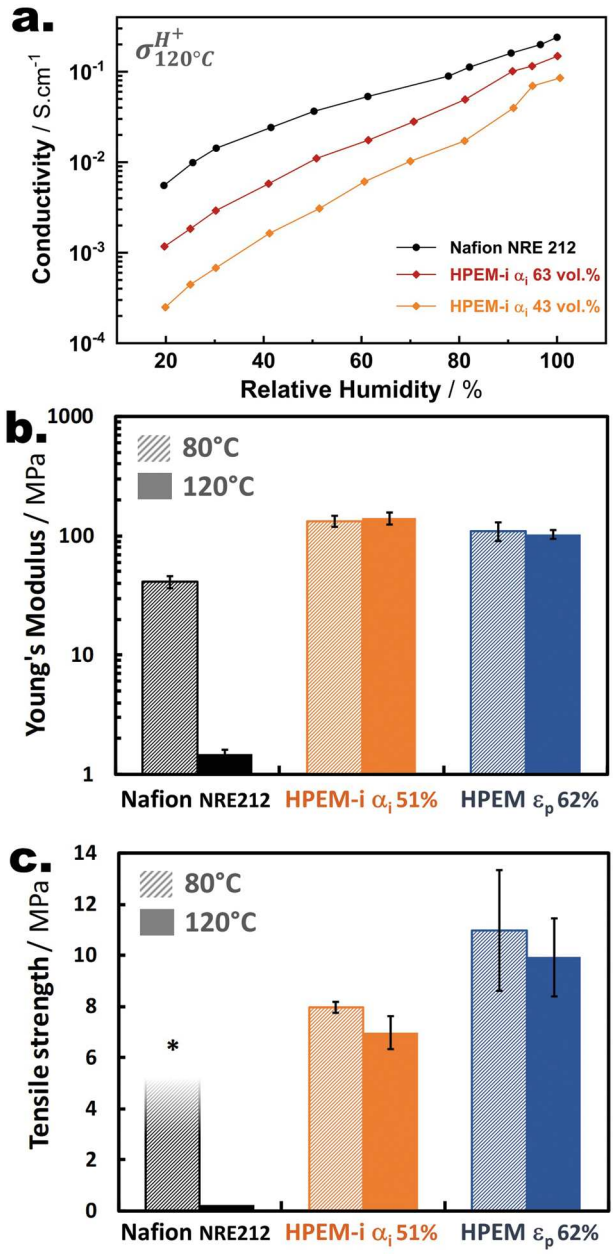

Figure 5. High temperature performances of HPEM-ionomer composites. a) Evolution of proton conductivity with relative humidity at 120 °C. Mechanical properties of hybrid, ionomer, and composites membranes at 80 and 120 °C measured by stress–strain analysis: b) Young's Modulus, c) ultimate tensile strength. * at least 4 MPa, elongation is too high to go to rupture (150% at 4 MPa).

properties, the ionomer network formed by impregnation ensures a relevant proton conductivity.

The mechanical and conduction properties of other representative composite PEM reported in the literature are listed in Table S2 and Section S7, Supporting Information. Several works reported tensile strengths ranging from 5 to 19 MPa for PVDF/sSiO_2 fibers mat incorporated or not into a PFSA matrix at room temperature, which is consistent with our values at 80 °C.[26,28,33,46,47] However, to the best of our knowledge, no previous studies reported the mechanical properties of hybrid PEM at 120 °C. Concerning the conductivity, Lee et al. measured an interesting conductivity of 12 mS cm^{-1} at 120 °C/40% RH for a composite membrane made of hybrid SPEEK/SiO_2 fibers embedded into a PFSA matrix, but the mechanical properties were not investigated.[46] Thus, HPEM-ionomer composite is a promising example of a composite membrane made with hybrid fibers showing both high mechanical and relevant conductive properties at elevated temperatures.

3. Conclusion

In this work, composite hybrid membranes were designed to be proton conductive and mechanically stable at 120 °C. First, a mat of hybrid nanofibers made of PVDF-HFP and sulfonated silica was synthesized via electrospinning. The polymer and silica domains were intimately mixed at the fiber scale with fractal interfaces, whose stability with temperature was improved by the removal of the PEG additive. On a larger scale, we found that the proton conductivity of the mat exponentially increased with its density, which was controlled through hot pressing. This allowed us to calculate an outstanding theoretical conductivity for a perfectly dense membrane: 1.8 S cm^{-1} at 80 °C/100% RH. However, the mats showed negligible proton conductivities at 120 °C; thus they were used as a mechanical reinforcement for composite membranes. The inter-fiber porosity of the mat was filled with a PFSA ionomer using a simple impregnation process, which allowed precise control of the nanofibers/ionomer volume ratio. The obtained composites membranes presented proton conductivities at 120 °C/90% RH of 100 and 40 mS cm^{-1} for an ionomer volume ratio of 66 vol% and 43 vol%, respectively. Moreover, the nanofibers mat acted as an extremely efficient mechanical reinforcement: the Young's modulus and the tensile strength of the composite membrane at 120 °C were, respectively, 95 and 35 times higher than that of the commercial Nafion 212 membrane.

This article demonstrates the importance of the efficient coupling between chemistry and processing in materials science. Indeed, coupling sol-gel and polymer chemistries with electrospinning and impregnation processes allowed for designing membranes with two different networks, ensuring superior conduction and mechanical performances. Overall, this strategy shows a simple and appealing approach to designing efficient proton exchanging membranes working at elevated temperatures. Moreover, the versatility of the method offers numerous tailoring possibilities; for instance, PVDF-HFP could be replaced with a functional amino-based polymer to form acid–base pairs along the hybrid nanofibers, which may improve the conductivity at high temperatures and low humidity.

4. Experimental Section

Chemicals: All chemicals were used as received. Tetraethyl orthosilicate (TEOS) (99%), poly(ethylene glycol) (PEG, M_n = 400 g mol^{-1}), *N*,*N*-dimethylformamide, hydrochloric acid (HCl, 37 wt%) and sodium hydroxide (99%) were purchased from Sigma Aldrich. 2–4(chlorosulfonylphenyl)ethyl trichlorosilane (CSPTC, 50% in methylene chloride) was purchased from ABCR. Poly(vinylidene

fluoride-co-hexafluoropropylene) (PVDF-HFP) (Solef 21 216) was provided by Solvay.

Synthesis of Hybrid Membranes: For the electrospinning of the HPEM, 10 wt% of PVDF-HFP was first dissolved in DMF before the addition of TEOS and CSPTC with a PDVF-HFP:TEOS:CSPTC mass ratio of 10:6:39. No water was added. The solution was kept at 70 °C for 3 h under vigorous magnetic stirring and was then cooled down to room temperature while maintaining the magnetic stirring overnight. The solution was then electrospun the following day.

For the precursor solution of HPEM-PEG containing poly(ethylene glycol) as an additive, PEG was added to the PVDF-HFP solution before TEOS and CSPTC.

A Nanospinner from Inovenso was used as the electrospinning setup for membrane synthesis. For a typical synthesis, 2 mL of the precursor solution was electrospun at 20 kV with a feed rate of 1.0 mL h^{-1} on a layer of non-adhesive paper attached to a rotating drum (5 cm radius, 400 rpm). The nozzle-collector distance was 15 cm and the relative humidity was maintained at 15%. After the electrospinning, membranes were removed from the paper and dried overnight at 70 °C. The membranes obtained were white, flexible and resistant, with a homogeneous aspect and a thickness of around 40 to 60 µm.

Membranes were placed between PTFE sheets and hot-pressed using a laminar press. The pressing time was fixed to 10 min and the temperature and pressure were varied from 80 to 90 °C and from 10 to 20 MPa, respectively, to control the porosity.

Synthesis of Composite Hybrid-Ionomer Membranes: To obtain composite HPEM-ionomer membranes, HPEM mats were soaked into a Nafion solution (20 wt% in a mixture of alcohols) and kept on a rotating mixer for 24 h at room temperature. Membranes were then removed from the solution and placed on a PTFE sheet. The excess solution was carefully removed using a plastic tool and the membranes were then dried overnight at 70 °C.

Characterization: SEM images were acquired on a Hitachi S-3400N operating at 6 kV, after deposition of a gold layer of 20 nm on the samples. The fiber diameter was measured using ImageJ software on at least 50 fibers. EDX Analyses were performed on the same instrument equipped with an EDX detector.

Elemental analyses were performed on an Elementar Vario Micro Cube to determine C wt% and S wt%, respectively, the mass content of carbon and sulfur. The IEC of the membranes was measured by indirect acid-base titrations. A sample of the membrane was first weighted, then soaked into an aqueous solution of sodium chloride (1 M NaCl) and gently stirred overnight at room temperature. The membrane was then removed and the aqueous solution was titrated with a NaOH solution; the evolution of pH was followed using a pH meter.

SAXS, with variable temperature and relative humidity, were performed using a home-made (CEA-Grenoble/IRIG/DePhy/MEM) SAXS line consisting in a FR591-3 kW rotating anode (Nonius) with Cu K_α radiation, a set of two Ni-filtered focusing mirrors (Xenocs) and a VÅNTEC-2000 2D detector (Brucker). The incident photon energy was adjusted to 8 keV, that is, a wavelength of $\lambda = 0.15118$ nm. The sample-to-detector distance was set to 186 cm for covering a ca. 0.15 to 3.5 nm^{-1} range of scattering-vector modulus. The 2D detector was off-centered to increase the q-range for the anisotropic samples. Silver behenate (AgBe, CAS number: [2489-05-6]) was used for the q-range calibration of the 2D detector. The complexes were sealed in home-made (copper brass-based) circular holders equipped with Kapton windows. 2D images were converted into radial averages over the image center to yield the scattered intensity $I(q)$ versus scattering-vector modulus q using the Datasqueeze software.

Stress–strain tests were performed on a DMA 850 from TA Instruments using a film clamp. The strain rate was fixed at 2% per minute. Young's moduli were calculated with a linear fit between 0.4% and 0.6% of elongation for all membranes. Each measure was repeated 3 to 5 times and mean values, as well as standard deviation was reported.

The porosity of the different separators was calculated from gravimetric measurements. The density of the membranes was first calculated following Equation (2):

$$d_{\mathrm{HPEM}} = \frac{m}{l \times L \times h} \tag{2}$$

with d_{HPEM} the density of the membranes in gram per centimeter cube, m the mass of the membrane in g, and l, L and h the width, length and thickness of the membrane in centimeters, respectively. The porosity ε_{p} was then calculated using Equation (3):

$$\varepsilon_{\mathrm{p}} = 1 - \frac{d_{\mathrm{HPEM}}}{d_{\mathrm{fiber}}} \tag{3}$$

with d_{fiber} the density of a hybrid fiber estimated to be 2.032 g cm^{-3} based on the densities of PVDF-HFP and SiO_2.

In-plane proton conductivity of the membranes was measured under nitrogen using a BT-512 In-Plane Membrane Conductivity Test System (BekkTech LLC). The dry dimensions of the membrane were considered for conductivity calculations. For measurements at 120 °C, the total absolute pressure in the cell was fixed at 2.5 bar. The conductivity values are given with a precision of 5.1% (see Section S8, Supporting Information, for more details).

Supporting Information

Supporting Information is available from the Wiley Online Library or from the author.

Acknowledgements

The authors thank SYMBIO for supporting JR's fellowship. In addition, the authors gratefully acknowledge Laurence Rozes and Mariette Lafont de Sentenac for DMA and Antoine Miche for XPS analysis and discussion, Isabelle Genois for EDX analysis, and Stéphane Lequien for his continual and determined help with the X-ray scattering.

Conflict of Interest

The authors declare no conflict of interest.

Data Availability Statement

The data that support the findings of this study are available from the corresponding author upon reasonable request.

Keywords

composite, high temperature, hybrid nanofiber, mechanical properties, PEMFC, perfluorosulfonic acid, proton transport

Received: July 20, 2022
Revised: October 25, 2022
Published online: December 1, 2022

[1] S. Khalili, E. Rantanen, D. Bogdanov, C. Breyer, *Energies* **2019**, *12*, 3870.
[2] X. Zhang, M. Zhang, Y. Deng, M. Xu, L. Artiglia, W. Wen, R. Gao, B. Chen, S. Yao, X. Zhang, M. Peng, J. Yan, A. Li, Z. Jiang, X. Gao, S. Cao, C. Yang, A. J. Kropf, J. Shi, J. Xie, M. Bi, J. A. van Bokhoven,

Y. W. Li, X. Wen, M. Flytzani-Stephanopoulos, C. Shi, W. Zhou, D. Ma, *Nature* **2021**, *589*, 396.
[3] X. Sun, S. C. Simonsen, T. Norby, A. Chatzitakis, *Membranes* **2019**, *9*, 83.
[4] N. A. M. Harun, N. Shaari, N. F. H. Nik Zaiman, *Int. J. Energy Res.* **2021**, *45*, 19671.
[5] M. Adamski, N. Peressin, S. Holdcroft, *Mater. Adv.* **2021**, *2*, 4966.
[6] Q. Yuan, Z. Fu, Y. Wang, W. Chen, X. Wu, X. Gong, D. Zhen, X. Jian, G. He, *J. Membr. Sci.* **2020**, *595*, 117516.
[7] B. A. Paren, B. A. Thurston, A. Kanthawar, W. J. Neary, A. Kendrick, M. Maréchal, J. G. Kennemur, M. J. Stevens, A. L. Frischknecht, K. I. Winey, *Chem. Mater.* **2021**, *33*, 6041.
[8] J. Chen, J. Cao, R. Zhang, J. Zhou, S. Wang, X. Liu, T. Zhang, X. Tao, Y. Zhang, *Membranes* **2021**, *11*, 826.
[9] J. Escorihuela, J. Olvera-Mancilla, L. Alexandrova, L. F. del Castillo, V. Compañ, *Polymers* **2020**, *12*, 1861.
[10] R. Sood, S. Giancola, A. Donnadio, M. Zatoń, N. Donzel, J. Rozière, D. J. Jones, S. Cavaliere, *J. Membr. Sci.* **2021**, *622*, 119037.
[11] C. Laberty-Robert, K. Vallé, F. Pereira, C. Sanchez, *Chem. Soc. Rev.* **2011**, *40*, 961.
[12] M. A. Imran, T. Li, X. Wu, X. Yan, A. S. Khan, G. He, *Chin. J. Chem. Eng.* **2020**, *28*, 2425.
[13] J. Escorihuela, R. Narducci, V. Compañ, F. Costantino, *Adv. Mater. Interfaces* **2019**, *6*, 1801146.
[14] X. Zhang, D. Trieu, D. Zheng, W. Ji, H. Qu, T. Ding, D. Qiu, D. Qu, *Ind. Eng. Chem. Res.* **2021**, *60*, 11086.
[15] S. Ryu, B. Lee, J. H. Kim, C. Pak, S. H. Moon, *Int. J. Energy Res.* **2021**, *45*, 19136.
[16] E. Bakangura, L. Wu, L. Ge, Z. Yang, T. Xu, *Prog. Polym. Sci.* **2016**, *57*, 103.
[17] G. Zhao, H. Zhao, X. Zhuang, L. Shi, B. Cheng, X. Xu, Y. Yin, *J. Mater. Chem. A* **2021**, *9*, 3729.
[18] Z. Zakaria, N. Shaari, S. K. Kamarudin, R. Bahru, M. T. Musa, *Int. J. Energy Res.* **2020**, *44*, 8255.
[19] J. Li, H. Tang, Z. Wang, M. Pan, *J. Power Sources* **2013**, *234*, 333.
[20] T. Hoshino, K. Hayashi, W. Sakamoto, T. Yogo, *J. Membr. Sci.* **2016**, *502*, 133.
[21] M. Takemoto, K. Hayashi, S. ichi Yamaura, W. Zhang, W. Sakamoto, T. Yogo, *Polymer* **2017**, *120*, 264.
[22] M. Hattori, S. ichi Yamaura, W. Zhang, W. Sakamoto, T. Yogo, *J. Membr. Sci.* **2015**, *488*, 166.
[23] G. Liu, W. C. Tsen, S. Wen, *Mater. Des.* **2020**, *193*, 108806.
[24] H. Wang, X. Wang, T. Fan, R. Zhou, J. Li, Y. Long, X. Zhuang, B. Cheng, *Solid State Ionics* **2020**, *349*, 115300.
[25] N. R. Mojarrad, B. Iskandarani, A. Taşdemir, A. Yürüm, S. A. Gürsel, B. Y. Kaplan, *Int. J. Hydrogen Energy* **2021**, *46*, 13583.
[26] V. Maneeratana, J. D. Bass, T. Azaïs, A. Patissier, K. Vallé, M. Maréchal, G. Gebel, C. Laberty-Robert, C. Sanchez, *Adv. Funct. Mater.* **2013**, *23*, 2872.
[27] K. Valle, P. Belleville, F. Pereira, C. Laberty, C. Sanchez, J. Bass, WO 2011/124622 A2, **2011**.
[28] O. Sel, T. Azais, M. Maréchal, G. Gébel, C. Laberty-Robert, C. Sanchez, *Chem. - Asian J.* **2011**, *6*, 2992.
[29] L. Dos Santos, S. Rose, O. Sel, M. Maréchal, H. Perrot, C. Laberty-Robert, *J. Membr. Sci.* **2016**, *513*, 12.
[30] L. Dos Santos, O. Dubrunfaut, J. C. Badot, C. Laberty-Robert, *J. Phys. Chem. C* **2016**, *120*, 6963.
[31] L. Dos Santos, M. Maréchal, A. Guillermo, S. Lyonnard, S. Moldovan, O. Ersen, O. Sel, H. Perrot, C. Laberty-Robert, *Adv. Funct. Mater.* **2016**, *26*, 594.
[32] S. M. Slade, T. R. Ralph, C. P. De León, S. A. Campbell, F. C. Walsh, *Fuel Cells* **2010**, *10*, 567.
[33] L. Dos Santos, D. Powers, R. Wycisk, P. N. Pintauro, *Membranes* **2020**, *10*, 250.
[34] A. K. Maurya, L. Weidenbacher, F. Spano, G. Fortunato, R. M. Rossi, M. Frenz, A. Dommann, A. Neels, A. Sadeghpour, *Nanoscale* **2019**, *11*, 7176.
[35] A. K. Maurya, E. Mias, J. Schoeller, I. E. Collings, R. M. Rossi, A. Dommann, A. Neels, *Nanoscale Adv.* **2022**, *4*, 491.
[36] H. Jeon, J. Choi, M. H. Ryou, Y. M. Lee, *ACS Omega* **2017**, *2*, 2159.
[37] A. Gogia, Y. Wang, A. K. Rai, R. Bhattacharya, G. Subramanyam, J. Kumar, *ACS Omega* **2021**, *6*, 4204.
[38] C. J. Brinker, *J Non Cryst Solids* **1988**, *100*, 31.
[39] S. Abbrent, J. Plestil, D. Hlavata, J. Lindgren, J. Tegenfeldt, Å. Wendsjö, *Polymer* **2001**, *42*, 1407.
[40] Z. Shang, R. Wycisk, P. Pintauro, *Energies* **2021**, *14*, 6709.
[41] Z. Siroma, R. Kakitsubo, N. Fujiwara, T. Ioroi, S. ichi Yamazaki, K. Yasuda, *J. Power Sources* **2009**, *189*, 994.
[42] S. Feng, G. A. Voth, *J. Phys. Chem. B* **2011**, *115*, 5903.
[43] N. Agmon, *Chem. Phys. Lett.* **1995**, *244*, 456.
[44] S. Kundu, L. C. Simon, M. Fowler, S. Grot, *Polymer* **2005**, *46*, 11707.
[45] M. Laporta, M. Pegoraro, L. Zanderighi, *Macromol. Mater. Eng.* **2000**, *282*, 22.
[46] C. Lee, S. M. Jo, J. Choi, K. Y. Baek, Y. B. Truong, I. L. Kyratzis, Y. G. Shul, *J. Mater. Sci.* **2013**, *48*, 3665.
[47] H. Wang, X. Li, X. Zhuang, B. Cheng, W. Wang, W. Kang, L. Shi, H. Li, *J. Power Sources* **2017**, *340*, 201.